Journal of Materials Chemistry A

Accepted Manuscript

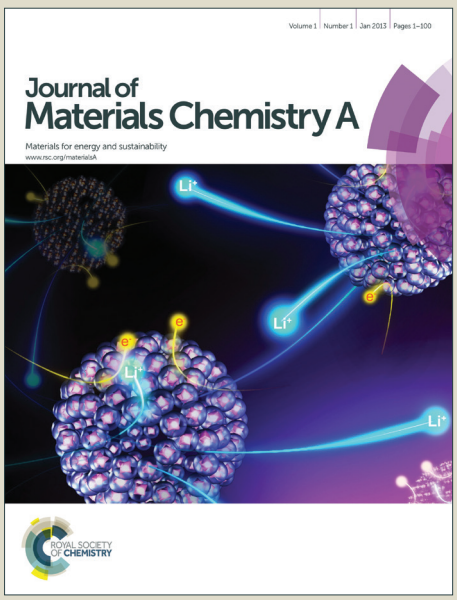

ROYAL SOCIETY OF CHEMISTRY

www.rsc.org/materialsA

Journal Name

RSCPublishing

ARTICLE

Fabrication of high-density silver nanoparticles on the surface of alginate microspheres for application in catalytic reaction†

Cite this: DOI: 10.1039/x0xx00000x

Received 00th January 2014,
Accepted 00th January 2014

DOI: 10.1039/x0xx00000x

www.rsc.org/

Jun You, Chengcheng Zhao, Jinfeng Cao, Jinping Zhou*, and Lina Zhang

In this work, we presented an environmentally-friendly approach for the immobilization of high-density silver nanoparticles (Ag NPs) on the negatively charged surface of alginate (AL) microspheres. Quaternized cellulose (QC)-Ag nanocomposites are subsequently deposited onto the surface of AL microspheres through the electrostatic interaction between QC and AL. The density of Ag NPs immobilized on the surface of AL microspheres could be altered by varying the Ag content in QC-Ag nanocomposites. Optical microscope, X-ray diffraction, X-ray photoelectron spectra, thermogravimetric analysis, transmission electron microscopy and scanning electron microscopy were employed to follow all preparation steps and to characterize the resulting functional surfaces. The catalytic activity of the composite microspheres was evaluated by the reduction of *p*-nitrophenol to *p*-aminophenol by $NaBH_4$. The results demonstrated that the obtained microspheres exhibited excellent catalytic activity with a high reaction constant of 2.75 min^{-1}. This was a significant enhancement compared to other Ag catalysts reported in the literature.

1. Introduction

In recent years, there has been increased interest in the development of Ag/polymer composites due to their significant potential for application in the fields of sensors,[1,2] biochemistry,[3,4] photoelectric[5,6] and catalysis.[7-9] The polymer matrixes not only provides better stabilization for Ag NPs, but also endows them with a variety of new functions. For instance, Lu et al. immobilized high-density Ag NPs onto the surface of a temperature-sensitive polymer film and the particle spacing of the supported Ag NPs was shown to be easily adjustable using temperature-controlled substrate shrinkage.[10] A variety of approaches have been reported for the synthesis of Ag/polymer composites, such as the direct blending of pre-made Ag NPs with a polymer matrix using a common blending solvent or through in situ reduction of silver salt dispersed in polymeric matrix with the use of an external reducing agent.[11-13] However, in most cases, Ag NPs were mainly embedded inside the polymer matrix, which were unfavorable for the application in the fields such as catalysis and bacteriostasis [14,15]

The direct deposition of metal nanoparticles on the surface of solid matrix has been regarded as one of the most efficient way to solve the above problem. Several routes have been proposed for the fabrication of core-shell composites, including sputtering methods,[16] self-assembly[17,18] and electroless plating.[19,20] Self-assembly has presented advantages over other methods due to its environment-friendly process, ability to create uniform coatings over small areas, simple equipment, low cost and ease of morphological manipulation for metal nanoparticles.[21,22] More recently, Goli et al. reported a simple and green method for the attachment of Ag NPs to polypropylene fibers mediated by electrostatic interactions between the positively charged surface and the negatively charged Ag NPs. The Ag/polymer composites exhibited excellent antibacterial activity with 100% removal efficiency.[23] However, the degree of surface coverage was relatively low in most cases. Usually, higher Ag content of the hybrid materials means higher catalytic and bacteriostatic activities. To achieve an exciting property, it is significant importance to improve the degree of the surface coverage of Ag NPs on the polymer substrate.[18] On the other hand, consideration should also be given to the stability of Ag coating under different chemical conditions (such as acid/base), due to the dissociation of Ag NPs from the surface may also reduce the properties of the hybrid materials. In order to accomplish these purposes, a suitable capping agent should be selected for the preparation of charged silver colloidal solution with high Ag content.

As one of the most common polysaccharides, cellulose is an almost inexhaustible polymeric raw material with fascinating structure and properties.[24] However, the applications of cellulose have previously been restricted owing to its insolubility in common solvents. Therefore, chemical modification continue to play an important role in improving cellulose utilization in polymeric materials.[25,26] Thus, novel cationic polyelectrolyte, quaternized cellulose (QC), was homogeneously synthesized from cellulose in NaOH/urea aqueous solution for wide application.[27-31] More recently, our work identified QC as an ideal protective agent for Ag NPs due to the "electrosteric stabilization" provided by its cationic chains. The prepared QC-Ag nanocomposites showed a high Ag content of up to 93% with high stability in water.[32] In this work, a simple procedure was reported for the construction of core-shell Ag/polymer composites for improving coverage of Ag NPs by using

QC-Ag nanocomposites with high Ag content. Alginate (AL) microspheres were prepared and chosen as a model for the polymer matrix. Then, Ag NPs were immobilized effectively on the surface of AL microspheres through electrostatic interactions. Finally, a systematic investigation into the structure and catalytic activities of the QC-Ag coated AL microspheres (QC-Ag@AL) was conducted.

2. Experimental section

2.1. Materials

Cellulose was supplied by Hubei Chemical Fiber Group Ltd. (Xiangyang, China). The viscosity-average molecular mass (M_η) was determined to be 5.1×10^4 g/mol. Water-soluble QC was homogeneously synthesized in NaOH/urea aqueous solution,[27] the substitution degree (DS) of the quaternary ammonium group was determined to be 0.73 by using elemental analysis. All of the chemical regents ($AgNO_3$, $NaBH_4$, $CaCl_2$, sodium alginate etc.) were purchased from Sinopharm Chemical Reagent Co., Ltd., and used without further purification. Deionized water (Millipore) was used for all experiments.

2.2. Fabrication of AL microspheres

AL microspheres were prepared by an emulsification technique modified from the work of Zhu et al.[33] A well-mixed suspension containing 300 g of isooctane with 6.8 g of dissolved Span 85 was dispersed in a reactor. The resulting suspension was stirred at 800 rpm for 30 min. Subsequently, 200 g of the 1.5wt% sodium alginate solution was added into the suspension at room temperature. After stirring for 1 h at 1500 rpm, a solution containing 3.6 g of Tween 85 in 20 g of isooctane was added to the emulsion and stirred for another 1 h at the same speed to achieve stable water/oil emulsion droplets. Next, 20 mL of $CaCl_2$ solution (5 wt%) was added to promote the formation of ionic crosslinking, which was followed by stirring for 20 min. AL microspheres were washed with deionized water and then with alcohol five times to remove residual isooctane and surfactant. Finally, the AL microspheres were freeze-dried or stored in deionized water at 0–5 °C for further use.

2.3. Preparation of QC-Ag nanocomposites

Water-soluble QC-Ag nanocomposites were prepared in accordance with the previous work.[32] Briefly, 10 mL of 2.428×10^{-2} mol/L $AgNO_3$ solution was introduced into QC solution of a certain concentration under magnetic stirring, which was followed by the immediate addition of 7.5 mL of 0.1 mol/L $NaBH_4$ solution and further stirring for 1 h. The resulting solution was then dialyzed with regenerated cellulose tubes (M_w cutoff 8000) against distilled water for 5 days. The purified QC-Ag solution was lyophilized to obtain dry QC-Ag nanocomposites for further use. As listed in Table S1, five QC-Ag nanocomposites, coded as QC-Ag1 to QC-Ag5, were prepared by changing the initial QC concentration from 0.05 to 1 mg/mL.

2.4. Deposition of Ag NPs on AL microspheres

QC-Ag nanocomposite solution was prepared at a concentration of 2 mg/mL in deionized water. AL microspheres were then added and incubated at room temperature under magnetic stirring. Adsorption was allowed to proceed for 30 min, after which the suspension was centrifuged to separate the microspheres from the remaining unabsorbed QC-Ag solution. The resultant microspheres were ultrasonicated and rinsed copiously with deionized water to remove the loosely bound Ag NPs. Finally, the microspheres were freeze-dried or stored in deionized water at 0–5 °C. By changing the QC-Ag1 to QC-Ag5 nanocomposites, five composite microspheres were obtained and coded as QC-Ag1@AL to QC-Ag5@AL, respectively. According to the same method, AL microspheres were immersed into 2 mg/mL QC solution to prepare QC@AL microspheres.

2.5. Characterization

Optical micrographs of the microspheres were observed using an optical microscopy with a single reflex camera (EX20, Sunny, China). The content of Ag in the QC-Ag@AL microspheres was determined by using inductively coupled plasma mass spectrometry (ICP-MS) (Agilent, Tokyo, Japan). FT-IR spectra were performed on a Nicolet 5700 Fourier transform infrared spectrometer. The test specimens were prepared by the KBr-disk method. X-ray diffraction (XRD) measurements were conducted on a XRD diffractometer (XRD-6000, Shimadzu, Japan). The patterns with Cu Kα radiation (λ = 0.15406 nm) at 40 kV and 30 mA were recorded in the region of 2θ from 30 to 85° with a step speed of 1°/min. Thermogravimetric analysis (TGA) was performed on a DSC-200PC (NETZSCH, Germany) in an air atmosphere at a heating rate of 15 °C/min from 30 to 800 °C. X-ray photoelectron spectra (XPS) were recorded on an ESCALAB 250Xi (Thermo Scientific) X-ray photoelectron spectrometer, using monochromatic Al Kα (1486.6 eV) radiation as the excitation source. Charge neutralization was required to prevent surface charge buildup. Binding energy was charge corrected to 284.6 eV for C1s. Scanning electron microscopy (SEM) images were taken on a field emission scanning electron microscope (FESEM: Zeiss Sigma). The samples were first sputtered with gold for SEM measurement. TEM images were observed on a JEM-2100 (HR) electron microscope, using an accelerating voltage of 200 kV. The freeze-dried QC-Ag@AL microspheres were embedded in epoxy resin Epon812 (Shanghai Bioscience, Shanghai, China). After that, the embedded specimen was sectioned by a LKB-8800 ultratome using a diamond knife to prepare approx.80 nm-thick sections. These samples were deposited on the copper grid for the further TEM measurement.

2.6. Catalytic activity assays

The catalytic activity of QC-Ag@AL microspheres was evaluated in the reduction of *p*-nitrophenol (Nip) to *p*-aminophenol (Amp) in a quartz cell at 15 °C. More specifically, 2 mL of *p*-nitrophenol solution (2×10^{-4}mol/L) was mixed with 1.87 mL of QC-Ag@AL microspheres dispersion. Subsequently, 0.13 mL of fresh $NaBH_4$ (3 mol/L) solution was added. Reactions were started after the addition of $NaBH_4$ solution, and they were monitored through the decreasing absorbance at 400 nm using UV-vis spectroscopy. The number of QC-Ag@AL microspheres in the reaction solution was 9.3×10^3 particles per mL (about 45.8 mg/mL for QC-Ag5@AL).

3. Results and discussion

3.1. Preparation of QC-Ag NPs and AL microspheres

Ag NPs were synthesized by the chemical reduction of $AgNO_3$ with $NaBH_4$ in the presence of QC as a capping agent. For the hydrophilicity and strong electrostatic repulsion of the QC chains, QC-Ag nanocomposites owned high Ag content and stability, as well as good solubility in water (Table S1). Fig. 1 depicts the UV-vis spectra of Ag NPs prepared under different QC concentrations. In order to more clearly illustrate the difference of Ag content in QC-Ag nanocomposites, the concentration of QC for each sample was adjusted to 0.05 mg/mL. As shown in Fig. 1, the maximum absorbance of QC-Ag solution, which corresponds to the

concentration of Ag NPs,[34,35] increased rapidly with a decrease of QC concentration from 1 to 0.05 mg/mL. The absorption of QC-Ag5 solution was about 18 times higher than that of the QC-Ag1 solution. On the other hand, the absorption peak observed at ~400 nm in Fig. 1 corresponds to the typical surface plasmon resonance absorption of spherical Ag NPs with sizes ranging between 10 and 30 nm.[17,34] TEM image of QC-Ag1 NPs in the inset of Fig. 1 reveals an average size of 10.1 nm, which concurs with the UV-vis data.

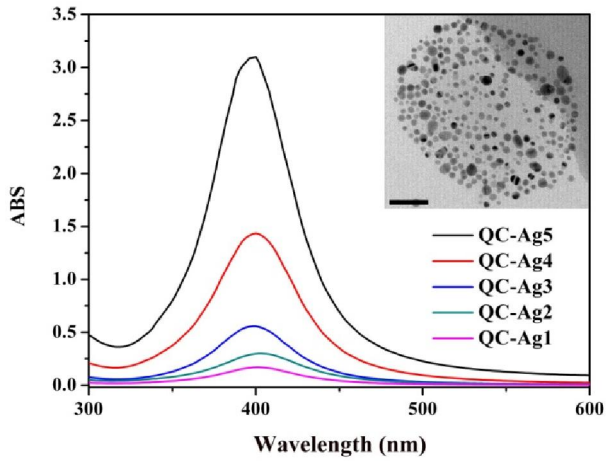

Fig. 1 UV-vis spectra of the prepared QC-Ag nanocomposites solution, the concentration of QC was adjusted to 0.05 mg/mL in each sample. Inset shows the TEM image of QC-Ag1 nanoparticles (scale bar: 50 nm).

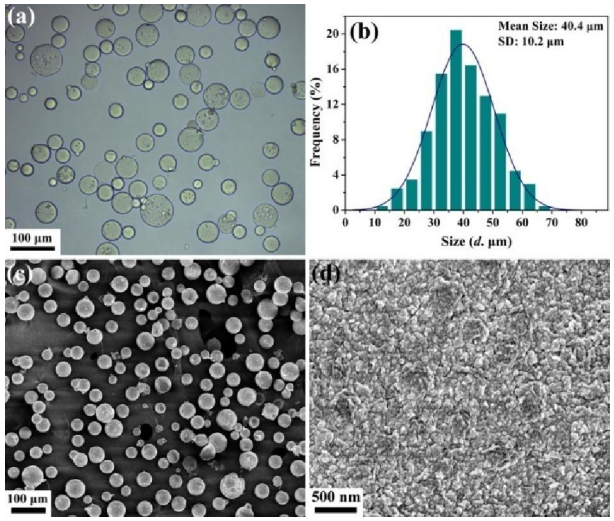

Fig. 2 Morphology of AL microspheres: (a) optical micrographs, (b) particle size histograms and (c, d) SEM images.

QC-Ag nanocomposites are positively charged; therefore they would preferably interact with the negatively charged surfaces. To this purpose, AL microspheres were prepared by an emulsification technique and chosen as the polymer matrix. The optical micrographs and the corresponding size distribution obtained by coulter counter measurements (*N*=200 particles counted) are shown in Fig. 2a and b. AL microspheres in a swollen state had an average diameter of around 40.4 μm. They exhibited spherical shape, and the size distribution fitted the Gaussian distribution. SEM images also proved AL microspheres had the spherical shape and homogeneous distribution (Fig. 2c). In addition, the microspheres exhibited well stability in deionized water and a smooth surface (Fig. 2d), which could be further utilized in QC-Ag assembly to construct core–shell Ag/Polymer composites.

3.2. Immobilization of Ag NPs on AL microspheres

Fig. 3 shows the optical micrographs and digital photographs of AL microspheres coated with QC and QC-Ag nanocomposites. Adsorption of QC-Ag nanocomposites could be easily monitored through color variations: both AL microspheres and QC@AL microspheres were colorless, whereas they assumed a yellow color after interaction with QC-Ag nanocomposites. Moreover, increasing Ag content resulted in a deep yellow/darker color of the QC-Ag@AL microspheres. This could be explained by the fact that the degree of the surface coverage of the AL microsphere gradually increased as we expected before.[23] Actually, from QC-Ag1@AL to QC-Ag5@AL microspheres, the Ag content was determined by ICP-MS to be 1.11, 2.03, 4.88, 9.70 and 12.5 wt%, respectively, which gradually increased with increasing Ag content of QC-Ag nanocomposites. On the other hand, the microspheres presented good spherical shape and no significant change in size, indicating that the coating process did not destroy the AL microspheres. Overall, the Ag NPs were successfully immobilized on the surface of the AL microspheres.

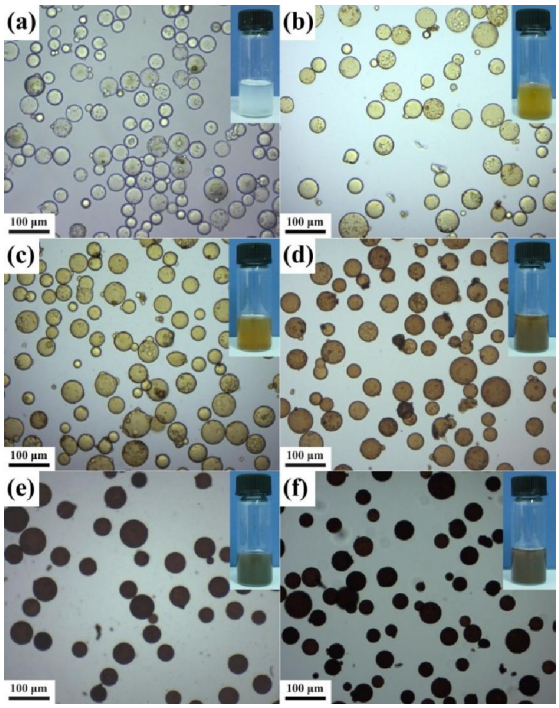

Fig. 3 Optical micrographs and photographs (Inset) of AL microspheres coated with (a) QC and (b) QC-Ag1, (c) QC-Ag2, (d) QC-Ag3, (e) QC-Ag4, (f) QC-Ag5 nanocomposites.

FT-IR measurements were performed to monitor the coating process of the AL microspheres. However, as shown in Fig. S1 in the Supporting Information, no obvious difference was observed. This may be attributed to the low content of QC/QC-Ag in the composite microspheres. XPS is one of the most sensitive surface analytical techniques, which could provide useful information on the nature of the surface composition of the materials.[36] Fig. 4a shows the wide-range XPS spectra of AL, QC@AL and QC-Ag5@AL

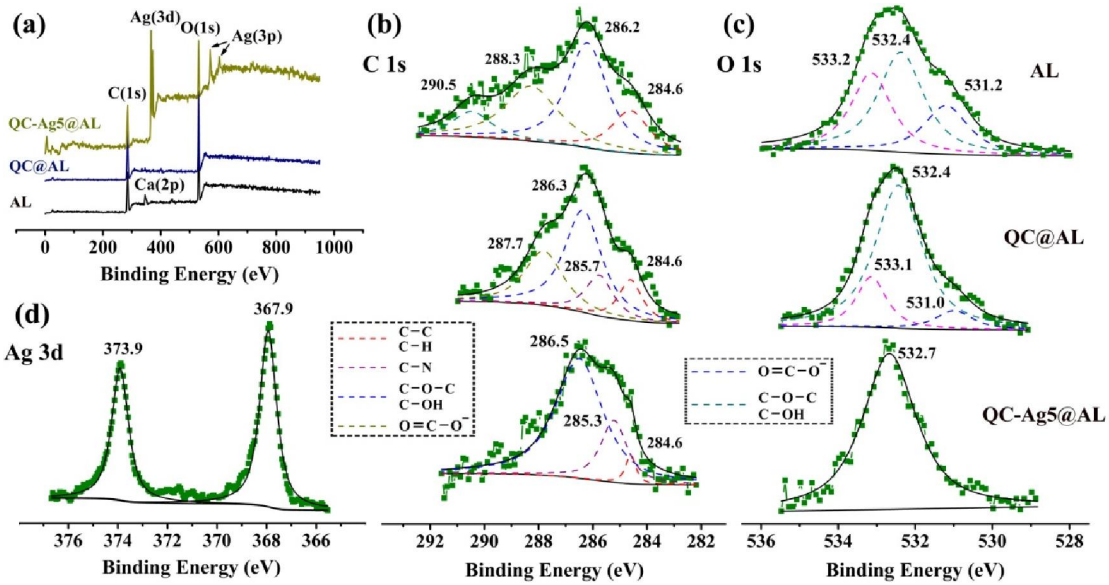

Fig. 4 XPS analysis of AL, QC@AL and QC-Ag5@AL microspheres.(a) The wide-range XPS spectra; (b) C1s spectra; (c) O1s spectra and (d) Ag3d spectrum.

microspheres. In the whole range of binding energy, AL microspheres had three clear peaks: C1s, O1s and Ca2p. The calcium element may come from the ionic crosslinking agent (Ca^{2+}) interact with carboxyl group. After immerging in the QC solution, the peak corresponding to Ca2p disappeared, indicating that the microsphere surface was successfully covered by QC. Upon coating with QC-Ag nanocomposites, two pairs of new peaks were observed, attributing to the Ag3d and Ag3p of the Ag NPs immobilized on the microspheres.

Fig. 4b and 4c illustrate the curve fitting of high-resolution multiplex scan spectra of C1s and O1s region in each microsphere. As shown in Fig. 4b, four peaks (284.6, 286.2, 288.3, and 290.5 eV) were observed in the spectrum of AL microspheres, corresponding to the carbon of alkyl (C−C/C−H, absorbed), alcoholic/ether (C−O−C/C−OH), carboxyl (COO^-) and the coordinated alcohol groups with Ca^{2+} ions, respectively.[37-39] In the spectrum of QC@AL microspheres, the peaks at 288.3 eV shifted to 287.7 eV, the peak at 290.5 eV disappeared and a new peak at 285.7 (C-N) was observed as compared to AL.[40] This clearly indicated that AL microspheres were covered by QC through electrostatic interaction. However, after coating with QC-Ag nanocomposites, the peak corresponding to the carboxyl group completely disappeared and the spectrum was similar to that of pure QC (Fig. S2). The thickness of Ag NPs shell in QC-Ag5@AL microspheres was determined to be ~150 nm (see TEM data below), which was far beyond the analytical depth of XPS measurement (5-10 nm). Thus, the signal detected by XPS may entirely come from QC-Ag nanocomposites. A similar phenomenon was observed in the spectra of the O1s region as shown in Fig. 4c. The results verified that Ag NPs were immobilized on the AL microspheres as a consequence of electrostatic interaction between QC and AL.

Fig. 4d shows the high-resolution multiplex scan spectrum of the Ag3d region of QC-Ag5@AL microsphere. The spectrum exhibited two specific peaks with binding energies of 367.9 and 373.9 eV, which were attributed to $Ag3d_{5/2}$ and $Ag3d_{3/2}$ electrons of Ag0. The spin energy separation was identified as 6.0 eV, which was characteristic of Ag NPs. Fig. 4d is the fine spectra of Ag, no information of silver oxide is found. The aforementioned peaks further confirmed the successful deposition of Ag NPs onto the surface of AL microspheres.

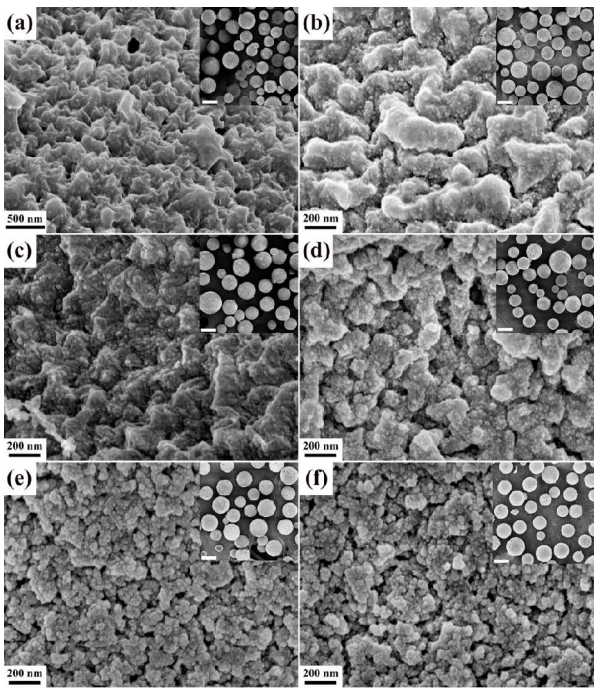

Fig. 5 SEM images of the surface of AL microspheres coated with (a) QC and (b) QC-Ag1, (c) QC-Ag2, (d) QC-Ag3, (e) QC-Ag4, (f) QC-Ag5 nanocomposites. Insert illustrates the morphology of the corresponding microspheres (scale bar: 50 μm).

3.3. Morphology and structure of QC-Ag@AL microspheres.

Fig. 5 shows SEM images of the AL microspheres coated with QC and QC-Ag nanocomposites. The inserts display the morphology of the corresponding microspheres, indicating their spherical shape as

well. Following coating with QC, the smooth surface of AL microspheres became rougher and small particulate structure could not be observed (Fig. 5a). Ag NPs could be clearly seen in Fig. 5b-f in the form of small particles, which revealed that they were immobilized and well dispersed on the surface of AL microspheres. Moreover, the coverage degree of Ag NPs on the matrix surface gradually increased with increasing Ag content in the coated QC-Ag nanocomposites. And finally, the inter-space between Ag NPs narrowed to form an almost continuous and compact Ag nanoshell (Fig. 5f). It is worth noting that the QC-Ag@AL microspheres were ultrasonicated in the preparation process for more than 1 h. Ag NPs still provided continuous coverage on the AL microsphere surface, which attested to the good adhesion between the Ag NPs and polymer substrate.[41] In many cases, an increase in the density of Ag NPs on the matrix surface always lead to obvious growth of the particle size.[42-44] In this work, the Ag NPs had already formed before the immobilization process. For the high protective efficiency of QC, Ag NPs maintained relative small particle size even under a very low polymer concentration. Therefore, the size of Ag NPs changed slightly as shown in Fig. 5.[31] The SEM results presented direct evidence for the successful immobilization of high-density Ag NPs on the surface of AL microspheres.

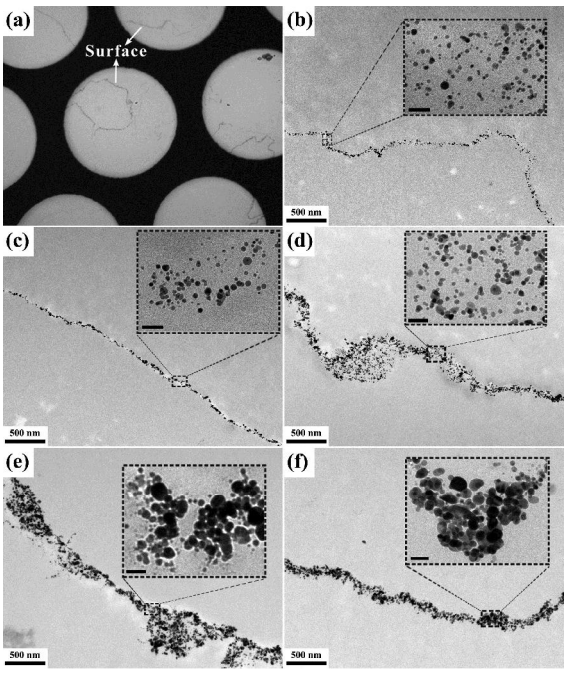

Fig. 6 (a) Optical micrographs of the ultrathin slices of the QC-Ag5@AL microspheres. TEM images of AL microspheres coated with (b) QC-Ag1, (c) QC-Ag2, (d) QC-Ag3, (e) QC-Ag4 and (f) QC-Ag5 nanocomposites. The scale bar in the insert is 50 nm.

Fig. 6a displays the optical micrographs of the ultrathin slices of the QC-Ag5@AL microspheres. A series of distinct lines could be observed which corresponded to the surface of microspheres. This clearly indicated that the Ag NPs were only immobilized on the surface of the substrate. TEM images of the area around the surface of the QC-Ag@AL microspheres are displayed in Fig. 6b-6f. An increase of Ag content in the coated QC-Ag nanocomposites led to a gradual increase in the thickness of the nanocomposites shell and the density of Ag NPs. On the other hand, spherical Ag NPs were well-dispersed on the surface of AL microspheres when the Ag NPs density was not too high (Fig. 6b-d). With an increase in the amount of immobilized Ag NPs on the surface, the inter-space between Ag NPs became narrower and a structure which was similar to the aggregate of Ag NPs occurred (Fig. 6e,f). A control experiment was performed to investigate the structure. As is well known, AL microsphere is a pH sensitive matrix that has a tendency to swell under basic conditions. As a result, AL microsphere surface will expand in all directions and carry the nanoparticles on its surface to a further contact.[10] If Ag NPs have formed aggregates, it is hard for us to separate them by this method. As shown in Fig. S3 of the Supporting Information, the color of the microspheres lightened after immersing in 0.1 M NaOH solution, indicating that Ag NPs immobilized on the surface of AL microsphere did not form aggregates. Moreover, it also indicated that the Ag coating on the microspheres was stable under acid and base conditions.

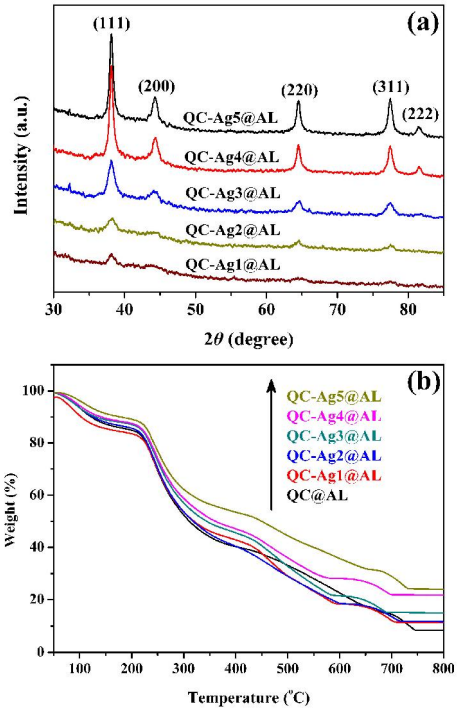

Fig. 7 (a) XRD patterns and (b) TG curves of QC@AL and QC-Ag@AL microspheres.

The deposition of Ag NPs could also be verified from the XRD data. As shown in Fig. 7a, five diffraction peaks were clearly observed at 2θ of 38.1, 44.3, 64.4, 77.4 and 81.6°, corresponding to the diffraction of the (111), (200), (220), (311) and (222) crystalline planes of cubic phase of Ag, respectively.[45] Ag_2O peaks were not observed in the diffraction patterns, indicating that the Ag NPs in QC-Ag@AL microspheres were not oxidated. Moreover, it was clear that the intensity of Ag crystal peaks gradually increased with the increase of Ag content in the coated QC-Ag nanocomposites, which indicated that the density of Ag NPs on the microsphere surface increased. This result was further supported by the TGA measurement as shown in Fig. 7b. The increase of remaining residue of QC-Ag@AL at 800 °C validated the increase of Ag content in composite microspheres. However, Ag NPs were only enriched on the microsphere surface and the thickness of the coating was only 50-150 nm. Thus, the great improvement of Ag NPs density on the surface slightly affected the Ag content in the microspheres. As a result, the increase of remaining residue at 800 °C was relative low, as compared with our previous work.[32] Moreover, the Ag content of

QC-Ag@AL microspheres calculated from the TG measurement matched well with those determined by ICP-MS.

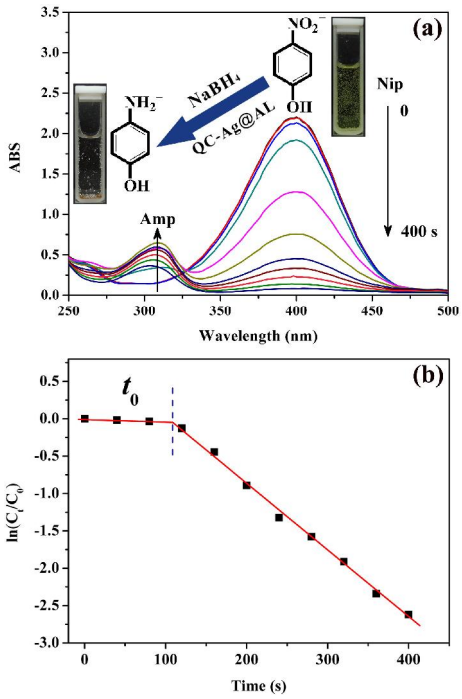

Fig. 8 (a) Variation in UV-visible absorption spectra for the Nip reduction from 0 to 400 s in the presence of QC-Ag1@AL microspheres, (b) linear relationship of $\ln(C_t/C_0)$ as a function of time.

3.4. Catalytic properties of QC-Ag@AL microspheres

The reduction of Nip to Amp by $NaBH_4$ was used as a model system to quantitatively evaluate the catalytic activity of the QC-Ag@AL microspheres. This reaction has become one of the model reactions for evaluating the activity of the catalysis in different substrates. The reduction is a thermodynamically feasible process involving E_0 for Nip/Amp = -0.76 V and H_3BO_3/BH_4^- = -1.33 V versus NHE, which is kinetically restricted. However, this reaction can be catalyzed by noble metal nanoparticles, and the reaction kinetics can be monitored by a simple way based on spectroscopic measurements.[46,47] The Nip/$NaBH_4$ mixture solution showed absorption at 400 nm, and the maximum absorption peak remains unaltered over time in the absence of catalysis. As shown in Fig. 8a, the addition of a small amount of QC-Ag@AL microspheres led to a rapid reduction of Nip as illustrated by a decrease in the absorption peak at 400 nm and concomitant appearance of a new peak at 300 nm corresponding to Amp (the reduction product of Nip). The color of the mixture solution faded by degrees and the absorption peak at 400 nm completely disappeared in about 400 s, indicating a near total conversion of Nip to Amp. It is worth noting that an initial induction time (t_0) before the onset of the rapid catalytic reaction was observed. It has been suggested that t_0 usually relates to the diffusion-controlled adsorption of substrates (combined with $NaBH_4$) onto the metal NPs surface.[48,49]Moreover,a linear correlation in the $\ln(C_t/C_0)$ versus reduction time t plot was observed as shown in Fig. 8b, indicating that the reaction followed a first-order rate law.

Fig. 9 illustrates a comparison of the catalytic activity of different QC-Ag@AL microspheres. In order to more clearly illustrate the difference between them, the concentration of each sample was adjusted to the same (9.3×10^3 microspheres per milliliter). QC@AL microspheres were used as a control and no reaction was observed. A slight decrease in the absorption was mainly attributed to the adsorption of Nip ion by the polymer matrix.[14] As shown in Fig. 9a, an increase in Ag density on the microsphere surface led to both an increase in the catalytic reaction rate and an obvious decrease in t_0. This could be explained by the fact that the rate constant (k) value generally increased with an increase of the catalyst concentration for the heterogeneous catalysis.[50] Linear relationships between $\ln(C_t/C_0)$ and reaction time were further obtained (Fig. 9b), where k of the highest value was calculated as 2.75 min^{-1} for QC-Ag5@AL. As summarized in Table 1, the reaction constant is much larger than those reported in the recent literatures with other Ag catalysts.

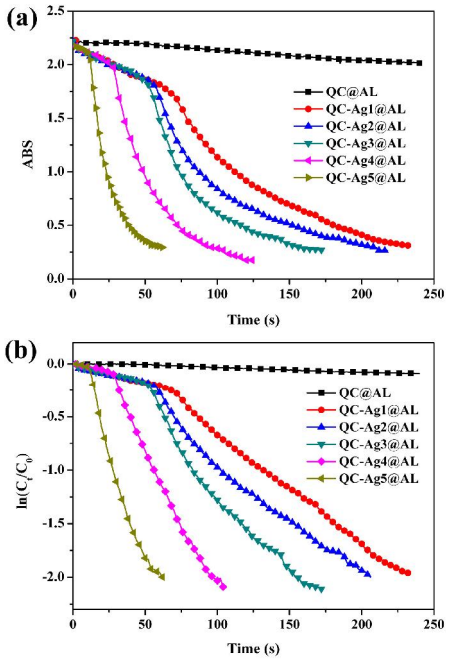

Fig. 9 (a) Extinction at the peak position for Nip (400 nm) as a function of time in the presence of QC-Ag@AL microspheres. (b) The relationship between $\ln(C_t/C_0)$ and reaction time with different QC-Ag@AL microspheres.

Table 1 A comparison of the kinetic constant (k) value for $NaBH_4$ reducing Nip as reported in recent literature using different catalysts based on Ag NPs

Catalyst	c_{NaBH_4} (M)	$c_{Catalyst}$ (mg/L)	k (min^{-1})	Ref.
Ag@AMH	0.05	4 beads	0.27	12
Cellulose/Ag	0.1	200	0.78	14
Ag/MFC	0.1	800	1.03	51
Fe_2O_3@Ag	0.14	/	0.9	52
AgNPs/ESM	0.03	1143	0.25	53
Ag-PPy	0.3	750	0.066	54
P2VP-Ag	0.013	thin film	0.03	55
QC-Ag@AL	0.1	45.8	2.8	This work

The catalytic stability of QC-Ag4@AL microspheres was further tested and the results are illustrated in Fig. S4a of the Supporting

Information. Nip was added to the cuvette after the reduction was over in each cycle, which allowed the reaction to proceed again. Interesting, the delay of reaction disappeared in the second and later cycles. It is suggested that the adsorption rate of Nip on the surface of catalysts is the predominant factor in the induction period. The adsorption of Nip might play an important role in activating the reaction.[49] The reduction started immediately because it had been activated in the first cycle. The reaction rate constant *k* for each cycle is calculated and illustrated in Fig. S4b of the Supporting Information. Compared with the first cycle, the *k* value increased obviously in the second cycle. As mentioned in Fig. S3, QC-Ag@AL microspheres swelled under basic condition, which carry the nanoparticles on its surface to a further contact. Thus the contact area between Ag NPs and Nip increased, which led to the increase in catalytic activity of QC-Ag microspheres. However, with further increasing the number of recycle times, the catalytic activity decreased. It suggested that the catalytic reduction product (Amp) can directly adsorb onto the QC-Ag@AL microspheres interface, because Amp have a strong affinity for the Ag NPs surfaces and electrostatic attraction for QC. This adsorption process may block the reactant (Nip) from reaching the Ag NPs surface, thus causing the reduction in catalytic activity for each cycle.[12,51]

4. Conclusions

Water-soluble Ag NPs were prepared by using QC as a protective agent, and AL microspheres were prepared through an emulsification technique. High-density of Ag NPs were further fixed to the surface of AL microspheres based on the high Ag content in QC-Ag nanocomposites and electrostatic interaction between AL and QC. The coverage degree of Ag NPs on the microsphere surface gradually increased with an increase of Ag content in the coated QC-Ag nanocomposites. QC-Ag@AL microspheres exhibited high catalytic activity for the reduction of Nip in $NaBH_4$ medium, attributing to the high-density of Ag NPs on the surface. This method provides a significant potential for application to the immobilization of Ag NPs on other negative charged surfaces.

Acknowledgements

This work was financially supported by National Natural Science Foundation of China (50973085 and 51273151), Program for New Century Excellent Talents in University (NCET-11-0415), National Basic Research Program of China (973 Program, 2010CB732203), Open Project of State Key Laboratory Cultivation Base for Nonmetal Composites and Functional Materials, and Fundamental Research Funds for the Central Universities.

Notes

Department of Chemistry and Key Laboratory of Biomedical Polymers of Ministry of Education, Wuhan University, 430072, China. E-mail address: zhoujp325@whu.edu.cn

†Electronic Supplementary Information (ESI) available: Conditions and results for the preparation of QC-Ag NPs; FT-IR spectra of the microspheres; XPS analysis of QC, effects of pH value on the morphology of the QC-Ag3@AL and QC-Ag5@AL microspheres and the catalytic stability of the QC-Ag4@AL microspheres See DOI: 10.1039/b000000x/

References

1 E. Park, O. S. Kwon, S. J. Park, J. S. Lee, S. You and J. Jang, *J. Mater. Chem.*, 2012, **22**, 1521-1526.
2 J. M. Köhler, A. März, J. Popp, A. Knauer, Is. Kraus, J. Faerber and C. Serra, *Anal. Chem.*, 2013, **85**, 313-318.
3 J. Song, H. Kang, C. Lee, S. H. Hwang and J. Jang, *ACS Appl. Mater. Interfaces*, 2012, **4**, 460-465.
4 J. Song, H. Kim, Y. Jang and J. Jang, *ACS Appl. Mater. Interfaces*, 2013, **5**, 11563-11568.
5 H. Kang, J. Yim, S. Jeong, J.-K. Yang, S. Kyeong, S.-J. Jeon, J. Kim, K. D. Eom, H. Lee, H.-I. Kim, D. H. Jeong, J.-H. Kim and Y.-S. Lee, *ACS Appl. Mater. Interfaces*, 2013, **5**, 12804-12810.
6 M. Park, J. Im, M. Shin, Y. Min, J. Park, H. Cho, S. Park, M.-B. Shim, S. Jeon, D.-Y. Chung, J. Bae, J. Park, U. Jeong and K. Kim, *Nature Nanotech.*, 2012, **7**, 803-809.
7 T. Yasukawa, H. Miyamura and S. Kobayashi, *J. Am. Chem. Soc.*, 2012, **134**, 16963-16966.
8 J. H. Lee, S. Kang, J. Y. Lee and J. H. Jung, *Soft Matter*, 2012, **8**, 6557-6563.
9 Y. Zheng and A. Wang, *J. Mater. Chem.*, 2012, **22**, 16552-16559.
10 Y. Lu, G. L. Liu and L. P. Lee, *Nano Lett.*, 2005, **5**, 5-9.
11 B. Xia, Q. Cui, F. He, L. Li, *Langmuir*, 2012, **28**, 11188-11194.
12 L. Ai, H. Yue and J. Jiang, *J. Mater. Chem.*, 2012, **22**, 23447-23453.
13 J. Park, Y. Lim, O. O. Park, J. K. Kim, J.-W. Yu and Y. C. Kim, *Chem. Mater.*, 2004, **16**, 688-692.
14 J. Wu, N. Zhao, X. Zhang and J. Xu, *Cellulose*, 2012, **19**, 1239-1249.
15 K. Varaprasad, Y. M. Mohan, K. Vimala and K. M. Raju, *J. Appl. Polym. Sci.*, 2011, **121**, 784-796.
16 A. Yasumori, H. Shinoda, Y. Kameshima, S. Hayashia and K. Okada, *J. Mater. Chem.*, 2001,**11**, 1253-1257.
17 E. Boanini, P. Torricelli, M. C. Cassani, G. A. Gentilomi, B. Ballarin, K. Rubini, F. Bonvicini and A. Bigi, *RSC Adv.*, 2014, **4**, 645-652.
18 A. Dong, Y. Wang, Y. Tang, N. Ren, W. Yang and Z. Gao, *Chem. Commun.* 2002, 350-351.
19 A. Radke, T. Gissibl, T. Klotzbücher, P. V. Braun and H. Giessen, *Adv. Mater.*, 2011, **23**, 3018-3021.
20 Y. Kobayashi, V. Salgueiriño-Maceira and L. M. Liz-Marzán, *Chem. Mater.*, 2001, **13**, 1630-1633.
21 Z. Tang, Z. Zhang, Y. Wang, S. C. Glotzer and N. A. Kotov, *Science*, 2006, **314**, 274-278.
22 M. Chirea, V. García-Morales, J. A. Manzanares, C. Pereira, R. Gulaboski, F. Silva, *J. Phys. Chem. B*, 2005, **109**, 21808-21817.
23 K. K. Goli, N. Gera, X. Liu, B. M. Rao, O. J. Rojas and J. Genzer, *ACS Appl. Mater. Interfaces*, 2013, **5**, 5298-5306.
24 D. Klemm, B. Heublein, H. P. Fink and A. Bohn, *Angew. Chem. Int. Ed.*, 2005, **44**, 3358-3393.
25 J. Tan, R. Liu, W. Wang, W. Liu, Y. Tian, M. Wu, Y. Huang, *Langmuir*, 2010, **26**, 2093-2098.
26 M. N. Nadagouda and R. S. Varma, *Biomacromolecules*, 2007, **8**, 2762-2767.
27 Y. Song, Y. Sun, X. Zhang, J. Zhou and L. Zhang, *Biomacromolecules*, 2008, **9**, 2259-2264.
28 Y. Song, H. Wang, X. Zeng, Y. Sun, X. Zhang, J. Zhou and L. Zhang, *Bioconjugate Chem.*, 2010, **21**, 1271-1279.
29 J. You, H. Hu, J. Zhou, L. Zhang, Y. Zhang and T. Kondo, *Langmuir*, 2013, **29**, 5085-5092.
30 Y. Song, J. Zhou, Q. Li, Y. Guo and L. Zhang, *Macromol. Biosci.*, 2009, **9**, 857-863.

31 J. You, J. Zhou, Q. Li and L. Zhang, *Langmuir*, 2012, **28**, 4965-4973.
32 J. You, M. Xiang, H. Hu, J. Cai, J. Zhou and Y. Zhang, *RSC Adv.*, 2013, **3**, 19319-19329.
33 H. Zhu, R. Srivastava and M. J. McShane, *Biomacromolecules*, 2005, **6**, 2221-2228.
34 S. Li, Y. Zhang, X. Xu and L. Zhang, *Biomacromolecules*, 2011, **12**, 2864-2871.
35 W. Haiss, N. T. K. Thanh, J. Aveyard and D. G. Fernig, *Anal. Chem.*, 2007, **79**, 4215-4221.
36 A. Vaish, V. Silin, M. L. Walker, K. L. Steffens, S. Krueger, A. A. Yeliseev, K. Gawrisch and D. J. Vanderah, *Chem. Commun.*, 2013, **49**, 2685-2687.
37 R. A. Bakare, C. Bhan and D. Raghavan, *Biomacromolecules*, 2014, **1**, 423-435.
38 J. P. Chen, L. Hong, S. Wu and L. Wang, *Langmuir*, 2002, **18**, 9413-9421.
39 S. K. Tam, J. Dusseault, S. Polizu, M. Ménard, J.-P. Hallé and L.Yahia, *Biomaterials*, 2006, **27**, 1296-1305.
40 A. Vinu, K. Ariga, T. Mori, T. Nakanishi, S. Hishita, D. Golberg and Y. Bando, *Adv. Mater.*, 2005, **17**, 1648-1652.
41 W. Wang, Y. Jiang, Y. Liao, M. Tian, H. Zou and L. Zhang, *J. Colloid Interface Sci.*, 2011, **358**, 567-574.
42 O. Siiman and A.Burshteyn, *J. Phys. Chem. B*, 2000, **104**, 9795-9810.
43 W. Cai, W. Wang, L. Lu and T. Chen, *Colloid Polym. Sci.*, 2013, **291**, 2023-2029.
44 F. M. Kelly and J. H. Johnston, *ACS Appl. Mater. Interfaces*, 2011, **3**, 1083-1092.
45 J. Li, W. Ma, C. Wei, J. Guo, J. Hu and C. Wang, *J. Mater. Chem.*, 2011, **21**, 5992-5998.
46 M. Schrinner, M. Ballauff, Y. Talmon, Y. Kauffmann, J. Thun, M. Moller, J. Breu, *Science*, 2009, **323**, 617-620.
47 J. Lee, J. C. Park and H. Song, *Adv. Mater.*, 2008, **20**, 1523-1528.
48 K. Kuroda, T. Ishida and M. Haruta, *J. Mol.Catal. A: Chem.*, 2009, **298**, 7-11.
49 J. Zeng, Q. Zhang, J. Chen and Y. N. Xia, *Nano Lett.*, 2010, **10**, 30-35.
50 S. Saha, A. Pal, S. Kundu, S. Basu, T. Pal, *Langmuir*, 2010, **26**, 2885-2893.
51 M. Zhu, C. Wang, D. Meng and G. Diao, *J. Mater. Chem. A*, 2013, **1**, 2118-2125.
52 K. Shin, J.-Y. Choi, C. S. Park, H. J. Jang and K. Kim, *Catal. Lett.*, 2009, **133**, 1-7.
53 M. Liang, R. Su, W. Qi, Y. Yu, L. Wang and Z. He, *J. Mater. Sci.* 2014, **49**, 1639-1647.
54 M. Chang, T. Kim, H.-W. Park, M. Kang, E. Reichmanis and H. Yoon, *ACS Appl. Mater. Interfaces*, 2012, **4**, 4357-4365.
55 L. Lin, K. Shang, X. Xu, C. Chu, H. Ma, Y.-I. Lee, J. Hao and H.-G.Liu, *J. Phys. Chem. B*, 2011, **115**, 11113-11118.

Graphical Abstract

Fabrication of high-density silver nanoparticles on the surface of alginate microspheres for application in catalytic reaction

Jun You, Chengcheng Zhao, Jinfeng Cao, Jinping Zhou,* and Lina Zhang

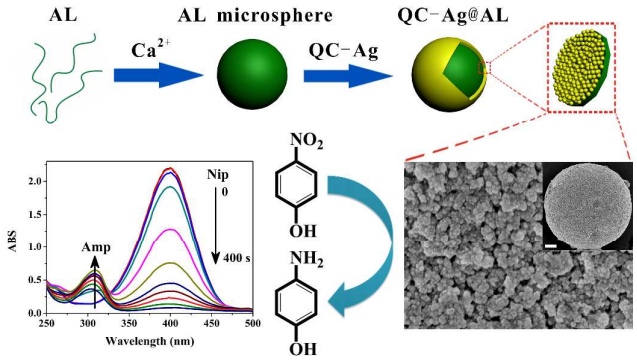

High-density of silver nanoparticles immobilized on the surface of alginate microspheres exhibit excellent catalytic activity for reduction of *p*-nitrophenol.

* Corresponding author. Tel.: +86 27 68752977. Fax: +86 27 68754067.

E-mail address: zhoujp325@whu.edu.cn (J. Zhou)